



VIIRS Suomi-NPP Level-2 Cirrus Reflectance Product (CLDCR_L2_VIIRS_SNPP) User Guide

Technical documentation

Bo-Cai Gao and Rong-Rong Li

Remote Sensing Division, Code 7230, Naval Research Lab, Washington DC

October 2020 (Version 1.3)

VIIRS SNPP L2 CIRRUS REFLECTANCE PRODUCT V001 - USER GUIDE

Revisions

Change record			
Version	Date	Author/changed by	Remarks
0.0	September/2019	Bo-Cai Gao (NRL/DC)	Initial draft
1.0	February/2020	Bo-Cai Gao (NRL/DC)	Change format
1.1	August/2020	Bo-Cai Gao (NRL/DC)	Product name change
1.2	September/2020	Bo-Cai Gao (NRL/DC)	Change descriptions on Quality assurance (QA)
1.3	October/2020	Bo-Cai Gao (NRL/DC)	Minor editing

The development of the VIIRS Cirrus Reflectance Algorithm was carried out at Remote Sensing Division, Naval Research Laboratory (NRL), 4555 Overlook Avenue, SW, Washington DC 20375 under a previous NASA contract awarded to NRL in DC.

Contacts

Readers seeking additional information about this study may contact the following researcher:

Bo-Cai Gao
Remote Sensing Division
Naval Research Laboratory
4555 Overlook Avenue, SW
Washington DC 20375 USA
Email: gao@nrl.navy.mil
Office: (202) 767-8252

Abstract

The purpose of this document is to provide technical information about the VIIRS Cirrus Cloud Reflectance Level-2 Product (CLDCR_L2_VIIRS_SNPP).

The CLDCR_L2_VIIRS_SNPP algorithm was adapted from the MODIS' MOD06CD algorithm with major modifications and improvements. VIIRS contains 11 narrow channels (M1 – M11) in the 0.4 – 2.5 μm solar spectral region, in addition to a number of IR emission channels. The M9 channel is specifically designed for detecting thin cirrus clouds. It is located within a strong atmospheric water vapor band absorption region. It is centered at 1.378 μm with a width of 15 nm. In comparison with the corresponding MODIS Channel 26, the VIIRS M9 channel is narrower and significantly more sensitive for cirrus detections. Because the radiances of the M9 channel over cirrus pixels are subjected to absorption by atmospheric water vapor molecules above and within cirrus, the water vapor absorption effect needs to be properly taken into consideration when using the M9 channel for quantitative removal of cirrus effects in other VIIRS channels in the 0.4 – 2.5 μm spectral range. The methodology of the CLDCR_L2_VIIRS_SNPP products can be found in the VIIRS/SOUMI-NPP Level-2 Cirrus Cloud Reflectance Algorithm Theoretical Basis Document (ATBD). In this ATBD, the empirical techniques for retrieving cirrus reflectances in the visible and NIR (0.4 – 1.0 μm), where ice particles within cirrus have negligible absorption effects, and shortwave IR (SWIR) (1.0 – 2.5 μm) where ice particle absorption effects are present, are described in details. The descriptions include all elements leading to the development of the operational VIIRS L2 cirrus reflectance algorithm, journal literature backing up the approach, theoretical descriptions on algorithm's physics and mathematical background, and sample retrieval results from VIIRS data.

TABLE OF CONTENTS

Revisions	2
Contact	4
Abstract.....	5
Table of contents	6
Software version identification	7
1. Introduction.....	7
The VIIRS cirrus reflectance algorithm.....	8
Processing the VIIRS Level-2 cirrus reflectance products	10
2. Technical information about CLDCR_L2_VIIRS_SNPP product file	11
3. References.....	12
Appendix 1: CLDCR_L2_VIIRS_SNPP product CDL file	13

Software version identification

The current version of the software is V1.3.

1. Introduction

Cirrus clouds generally consist of ice particles having different sizes and shapes. The "effective" particle sizes (radii of equivalent spheres) are usually greater than $5\ \mu\text{m}$. We illustrate the scattering and absorption properties of cirrus clouds through recent hyperspectral imaging data acquired with the AVIRIS-NG instrument from an ER-2 aircraft at an altitude of 20 km. Figure 1 shows a sample AVIRIS-NG spectrum (apparent reflectances) acquired over an area covered by thick cirrus on March 21, 2017. The VIIRS M1 – M11 channel positions and widths are marked in short and thick horizontal bars. In this thick cirrus spectrum, the atmospheric water vapor absorption bands centered near 0.94 , 1.14 , 1.38 , and $1.88\ \mu\text{m}$ are seen. The narrower atmospheric oxygen bands centered near 0.69 , 0.76 , and $1.26\ \mu\text{m}$ are also seen. In addition, a broad atmospheric ozone absorption band (Chapuis band) centered near $0.60\ \mu\text{m}$. For the cirrus spectrum, the reflectances of ice particles in the $0.4 - 1.0\ \mu\text{m}$ spectral region are nearly constant with wavelength, because ice particles are much larger than the wavelength and non-absorbing in this spectral region. Past $1.0\ \mu\text{m}$ one finds several ice absorption bands, for example those centered near 1.5 and $2.0\ \mu\text{m}$. Both the M10 ($1.61\ \mu\text{m}$) and M11 ($2.25\ \mu\text{m}$) channels are affected by ice absorption effects. Because M11 is centered near a local reflectance maximum, the overall ice absorption effect for the M11 channel can be smaller than that of the M10 channel. Weak ice absorptions occur near $1.24\ \mu\text{m}$ (M8) and $1.375\ \mu\text{m}$ (M9); the imaginary parts of the ice refractive index are about the same at both wavelengths. The measured reflectances at $1.375\ \mu\text{m}$ are smaller than those in the $0.4 - 1.0\ \mu\text{m}$ region mainly because of absorption by water vapor above and within cirrus clouds. These high-altitude water vapor absorption effects need to be accounted for in order to use the VIIRS M9 channel for quantitative retrieval of cirrus reflectances and for subsequent removal of cirrus effects in M1 – M8 channels. The use of the M9 channel for the removal of cirrus effects in M10 and M11 channels needs to take into considerations of the M9 water vapor absorption effects and the M10 and M11 ice absorption and scattering effects.

At present, our knowledge of cirrus ice particle size, shape, and orientation distributions, spatial variability, and scattering phase functions is not sufficient for reliable, routine modeling of cirrus reflectivity (Shiobara and Asano, 1994). Cirrus spatial inhomogeneity and adjacency effects (contamination of one pixel by photons scattered from neighboring pixels) are poorly treated in radiative transfer models. In view of these difficulties, we decided to use empirical relationships to characterize the main cirrus properties, and from these to develop an empirical cirrus reflectance

algorithm.

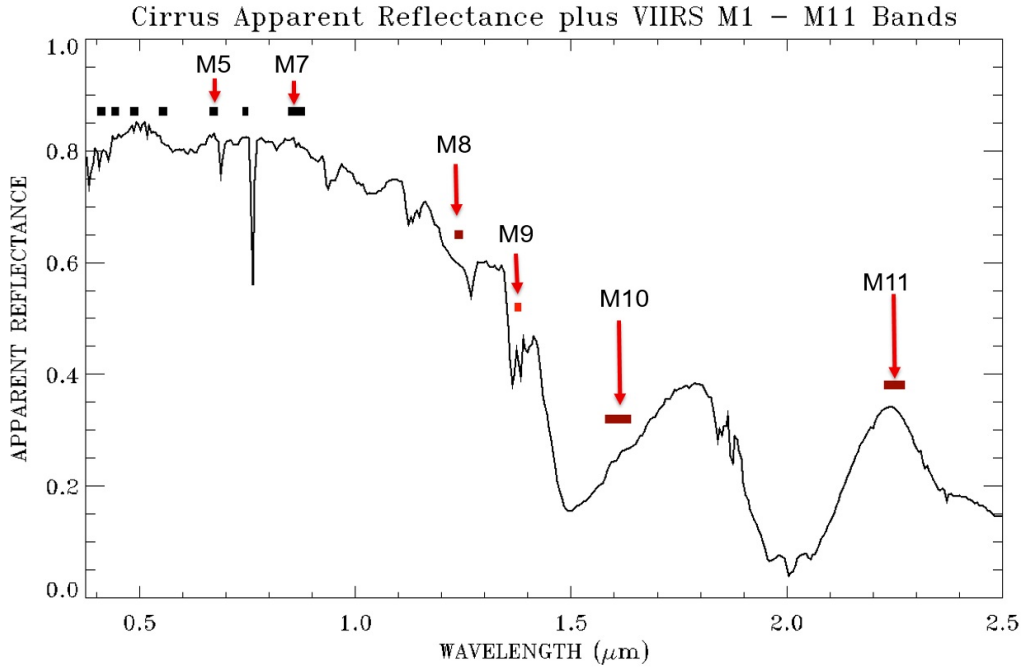


Fig. 1. A thick cirrus apparent reflectance spectrum with VIIRS M1 – M11 channels marked in short and thick horizontal bars.

The VIIRS cirrus reflectance algorithm

In the VIIRS Level-2 Cirrus Cloud Reflectance ATBD, detailed procedures have been described for the retrieving of cirrus reflectance data products from VIIRS L1B data and geolocation data. Below we use specific VIIRS case studies to further illustrate the cirrus reflectance derivation and the subsequent cirrus correction processes. Fig. 2a is the M5 "apparent reflectance" [$\rho^*(M5)$] image of a portion of a VIIRS scene. The "apparent reflectance" at the satellite for a given band is defined as $(\pi L / \mu_0 E_0)$, where L is the radiance measured by the satellite, μ_0 the cosine of solar zenith angle, and E_0 the extra-terrestrial solar flux at the top of the atmosphere. Both the high-altitude thin cirrus clouds and the low-altitude water clouds are seen. Fig. 2b is the corresponding M9 apparent reflectance [$\rho^*(M9)$] image. Only the high-altitude cirrus clouds are seen. The low-altitude water clouds and surface features are not seen because of strong absorption by water vapor beneath the cirrus clouds. Fig. 2c is the scatter plot of apparent reflectance images of M9 versus M5 bands. Pixels with least surface and low-altitude water cloud reflection contributions are located in the left-edge portion of the scatter plot. These pixels are used for the estimation of the SLOPE (shown in a short red line in the plot). Fig. 2d is the retrieved M5 band cirrus reflectance image, which is equal to $\{\rho^*(M5) - \rho^*(M9)/SLOPE\}$ (see the VIIRS Cirrus Reflectance ATBD for more detailed

descriptions). In order to test if the estimated M5 cirrus reflectances are correct, we show in Fig. 2e the cirrus corrected M5 band apparent reflectance image. By comparing Fig. 2e with Fig. 2a, it is seen that cirrus cloud features are properly removed in the Fig. 2e image. This demonstrates that the derived M5 band cirrus reflectances are sufficiently accurate for pixel-by-pixel cirrus removals.

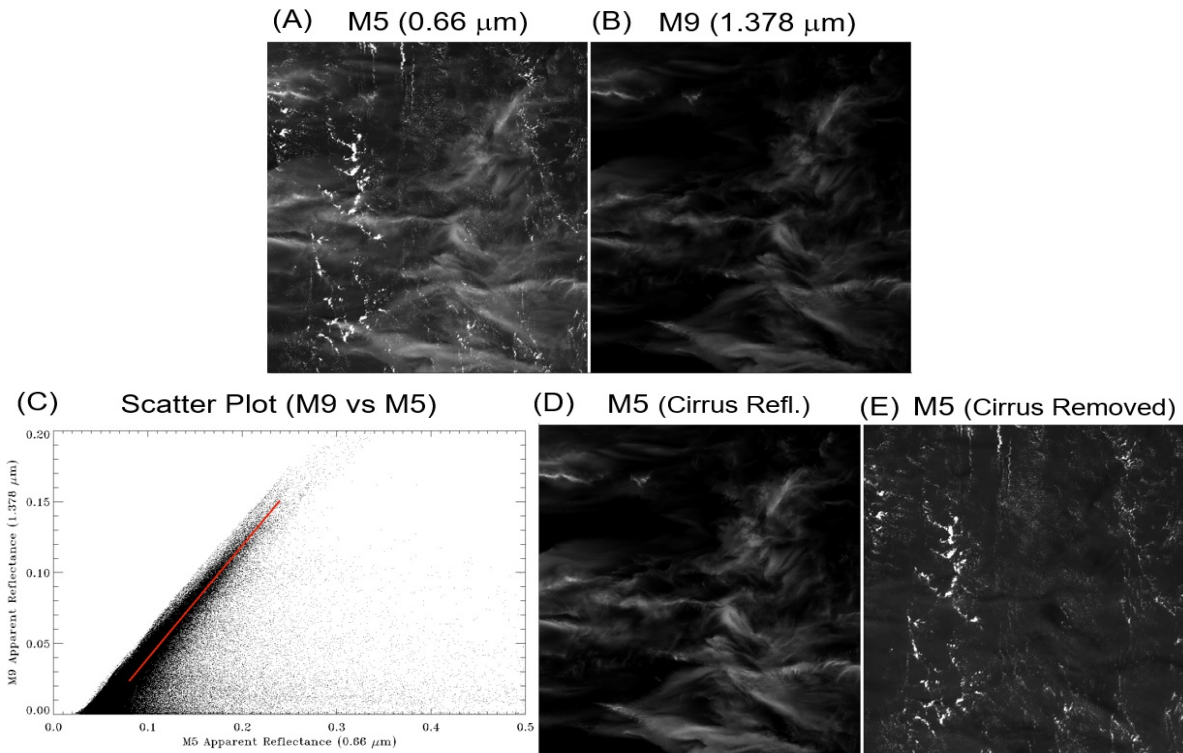


Fig. 2. (A) – A portion of a VIIRS M5 band apparent reflectance image, (B) – the M9 band apparent reflectance image, (C) – scatter plot of M9 versus M5 band images, (D) – the derived M5 band cirrus reflectance image, and (E) – the cirrus-removed M5 band apparent reflectance image.

Figure 3 shows another example of cirrus detections and corrections. Fig. 3a is a portion of a VIIRS RGB image acquired in January 2013 over the Red Sea area. The white cirrus features over land and water surfaces are seen. Fig. 3b is the corresponding M9 (1.378-μm) cirrus image. Here both the land and water surface features are not seen because of strong absorption near 1.378 μm by water vapor beneath cirrus. Fig. 3c is the cirrus-removed RGB image. The white cirrus features seen in Fig. 3a disappeared completely in the Fig. 3c image, which indicates the proper removal of thin cirrus scattering effects using the derived cirrus reflectances. In addition, the small greenish-colored water features in Red Sea are observed much better than those in the Fig. 3a original RGB image. The small bright cumulus clouds in the upper-left portion and the

lower-central portion of the scenes remain in the Fig. 3c image. There are dark features in the Fig. 3c image over desert areas. These features are related to cirrus shadows in the Fig. 3a RGB image, and they are not due to over-correction of cirrus effects. They are spatially displaced in comparison with the corresponding cirrus features in Fig. 3b.

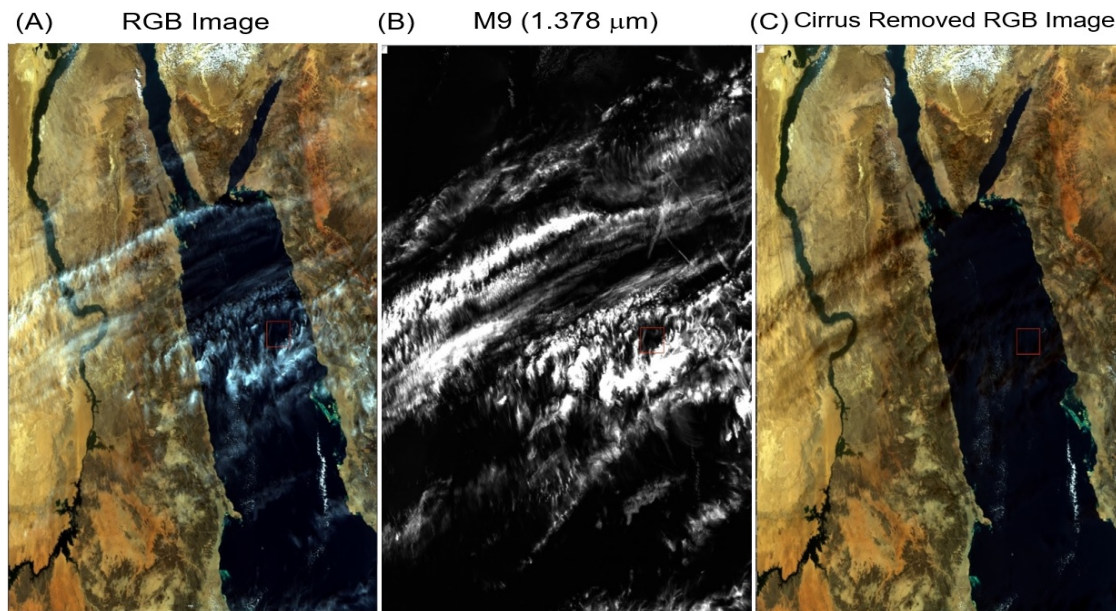


Fig. 3. (A) – A portion of a VIIRS RGB image over Red Sea and nearby areas, (B) – the M9 band apparent reflectance image, and (C) – the cirrus-removed RGB image.

Processing the VIIRS Level-2 cirrus reflectance products

The VSWIR Level-2 cirrus reflectance algorithm requires input data sets from the standard VSWIR L1b calibrated radiance and geolocation data cubes in netCDF4/HDF5 format. Specifically, the input data for a given VIIRS scene include: number of samples (the data points in the scan direction), number of lines (the data points in the flight direction), the apparent reflectance of M5 (0.66- μm), M8 (1.24- μm), M9 (1.378- μm), M10 (1.61- μm), and M11 (2.25- μm) channels; the brightness temperature of M14 (8.55- μm), M15 (10.76- μm), M16 (12.01- μm) channels; Latitude, longitude, surface elevation; solar zenith angle, solar azimuth angle, view zenith angle, and view azimuth angle.

The output data for a given VIIRS scene include: cirrus reflectance for VIS (visible) and NIR (near-IR) channels, cirrus reflectances for SWIR (shortwave IR) channels centered at 1.24, 1.61, and 2.25 μm , and the associated QA (quality assurance) parameter (which is required to generate the L2 global cirrus reflectance data products from the granule-based L2 data product). *End users of the VIIRS cirrus reflectance products are*

3. References

- Gao, B.-C., A. F. H. Goetz, and W. J. Wiscombe, Cirrus cloud detection from airborne imaging spectrometer data using the 1.38 μm water vapor band, *GRL.*, 20, 301-304, 1993.
- Gao, B.-C., and Kaufman, Y. J., Selection of the 1.375- μm MODIS channel for remote sensing of cirrus clouds and stratospheric aerosols from space, *J. Atm. Sci.*, 52, 4231-4237, 1995.
- Gao, B.-C., et al., Correction of thin cirrus path radiance in the 0.4-1.0 μm spectral region using the sensitive 1.375- μm cirrus detecting channel, *J. Geophys. Res.*, 103, 32169-32176, 1998.
- Gao, B.-C., Yang, P., Han, W., Li, R.-R., and Wiscombe, W. J., An algorithm using visible and 1.38- μm channels to retrieve cirrus cloud reflectances from aircraft and satellite data, *IEEE Trans. Geosci. Remote Sensing*, 40, 1659 – 1668, 2002.
- Gao, B.-C., and R.-R. Li, Removal of thin cirrus scattering effects in Landsat 8 OLI images using the cirrus detecting channels, *Remote Sensing*, 9, 834, 2017.
- Shiobara, M., and A. Asano, Estimation of cirrus optical thickness from sun photometer measurements, *JAM*, 33, 672-681, 1994.

Appendix 1. CLDCR_L2_VIIRS_SNPP Product CDL File

```
netcdf VCLDCR {
dimensions:
  number_of_lines = UNLIMITED; // either 3232 or 3248
  number_of_pixels = 3200;

// global attributes:
  :instrument = "VIIRS";
  :title = "VIIRS Cirrus Reflectance";
  :keywords_vocabulary = "NASA Global Change Master Directory (GCMD) Science Keywords";
  :license = "http://science.nasa.gov/earth-science/earth-science-data/data-information-policy/";

group: geophysical_data {
  variables:
    ushort Cirrus_Reflectance_VIS_NIR(number_of_lines, number_of_pixels) ;
      Cirrus_Reflectance_VIS_NIR:long_name = "M-bands VIS-NIR (0.4 - 1.0 micron) Cirrus
Reflectance" ;
      Cirrus_Reflectance_VIS_NIR: FillValue = 0s;
      Cirrus_Reflectance_VIS_NIR:scale_factor = 1.e-04;
      Cirrus_Reflectance_VIS_NIR:add_offset = 0.f;
    ushort Cirrus_Reflectance_SWIR_M08(number_of_lines, number_of_pixels);
      Cirrus_Reflectance_SWIR_M08:long_name = "M-band 08 Cirrus Reflectance";
      Cirrus_Reflectance_SWIR_M08: FillValue = 0s;
      Cirrus_Reflectance_SWIR_M08:scale_factor = 1.e-04;
      Cirrus_Reflectance_SWIR_M08:add_offset = 0.f;
    ushort Cirrus_Reflectance_SWIR_M10(number_of_lines, number_of_pixels);
      Cirrus_Reflectance_SWIR_M10:long_name = "M-band 10 Cirrus Reflectance";
      Cirrus_Reflectance_SWIR_M10: FillValue = 0s;
      Cirrus_Reflectance_SWIR_M10:scale_factor = 1.e-04;
      Cirrus_Reflectance_SWIR_M10:add_offset = 0.f;
    ushort Cirrus_Reflectance_SWIR_M11(number_of_lines, number_of_pixels);
      Cirrus_Reflectance_SWIR_M11:long_name = "M-band 11 Cirrus Reflectance";
      Cirrus_Reflectance_SWIR_M11: FillValue = 0s;
      Cirrus_Reflectance_SWIR_M11:scale_factor = 1.e-04;
      Cirrus_Reflectance_SWIR_M11:add_offset = 0.f;
    byte Cirrus_Reflectance_QA(number_of_lines, number_of_pixels);
      Cirrus_Reflectance_QA:long_name = "Cirrus Reflectance QA";
      Cirrus_Reflectance_QA: FillValue = -1b;
      Cirrus_Reflectance_QA:scale_factor = 1.0;
      Cirrus_Reflectance_QA:add_offset = 0.f;
  } // group geophysical_data
}
```